

Seismic performance of cold-formed steel bolted moment connections with bolting friction-slip mechanism

Jun Ye¹, Seyed Mohammad Mojtabaei^{2*}, Iman Hajirasouliha²

¹Department of Architecture and Civil Engineering, University of Bath, UK

² Department of Civil and Structural Engineering, University of Sheffield, UK

* Corresponding author. E-mail: smmojtabaei1@sheffield.ac.uk;

Abstract:

Typical cold-formed steel (CFS) moment-resisting connections generally have relatively low ductility and energy dissipation capacity as a result of low local/distortional buckling resistance of thin-walled CFS elements, and therefore, may not be suitable for seismic applications. To address this issue, a comprehensive analytical study is presented on the seismic performance of CFS bolted beam-to-column connections with fiction-slip mechanism aiming to obtain more efficient design solutions suitable for CFS frames in seismic regions. Experimentally validated finite element (FE) models in ABAQUS are used to predict the hysteretic behaviour and failure of a range of CFS connections by taking into account the characteristics of the bolting system as well as nonlinear material properties and geometrical imperfections. The developed models are then used to investigate the effects of CFS beam cross-sectional shape and classification, bolt configuration, and slip resistance on the seismic performance of the connections. It is shown that using bolting friction-slip mechanism can significantly increase (up to 200%) the ductility, energy dissipation capacity and damping coefficient of the connections especially for CFS beams with thinner plates (class 3 and 4). Based on the results, the best design configurations are identified to improve the cyclic response of the CFS connections under strong earthquakes. While conventional bolted moment connections with class 3 and 4 beam cross-sections generally do not satisfy the AISC requirements for intermediate and special moment frames, it is shown that

optimum designed connections with bolting friction-slip mechanism can be efficiently used in high seismic regions.

Key words: Cold-formed Steel; Seismic Performance; Friction-slip Mechanism; Bolted Moment Connection; Cyclic behaviour; Optimum Design

1. Introduction

Cold-formed steel (CFS) sections are produced by rolling or pressing of thin-walled steel sheets to form open cross sectional shapes at ambient temperature (cold working). In general, CFS elements can be more economical and efficient compared to their hot-rolled counterparts due to their inherent advantages such as high strength-to weight ratio, ease and speed of construction, and especially higher flexibility in manufacturing various cross-sectional profiles and sizes [1-3]. Traditionally, application of CFS sections as main structural components has been restricted to the conventional shear walls (or stud wall) systems. The seismic behaviour of shear walls with different configurations and bracing systems has been investigated experimentally by several full-scale cyclic and monotonic tests [4-6]. While there is a consensus that shear wall systems can generally carry lateral and vertical loads up to the limits required by most seismic codes, typical CFS shear wall systems may not provide high ductility mainly due to the premature buckling of the thin-walled stud elements [7].

Previous studies indicated that, in general, CFS bolted moment connections are capable of providing sufficient flexural stiffness, ultimate strength, and deformation capacity for multi-storey moment-resisting frames [3, 8]. However, by increasing the width-to-thickness ratio of CFS plates, the typical CFS bolted moment connections may not be able to provide enough energy dissipation capacity and ductility [9]. This limitation is a major obstacle for widespread application of CFS moment-resisting frames in seismic regions.

Seismic design of structures normally relies on inelastic deformations through hysteretic behaviour, leading to damage and permanent deformation of structural elements, and hence high repair costs, following a strong earthquake event. In steel construction, using friction-slip mechanism is known as an alternative seismic design approach, implemented to absorb the energy of the earthquake and consequently reduce and control the damage to the structural elements [10]. In general, development of plasticity in the connection zone of CFS moment-resisting frames cannot be easily achieved due to the higher vulnerability of thin-walled elements (i.e. with large width-to-thickness ratio) to local/distortional buckling compared to their hot-rolled counterparts [9]. Therefore, accommodating friction-slip mechanism in the CFS bolted moment connections to dissipate the earthquake input energy can provide a practical solution to improve the seismic performance of CFS moment-resisting frames. In practice, friction-slip mechanism can be easily activated in bolted moment connection by providing appropriate bolt tightening and detailing [10], which is presented schematically in Fig. 1.

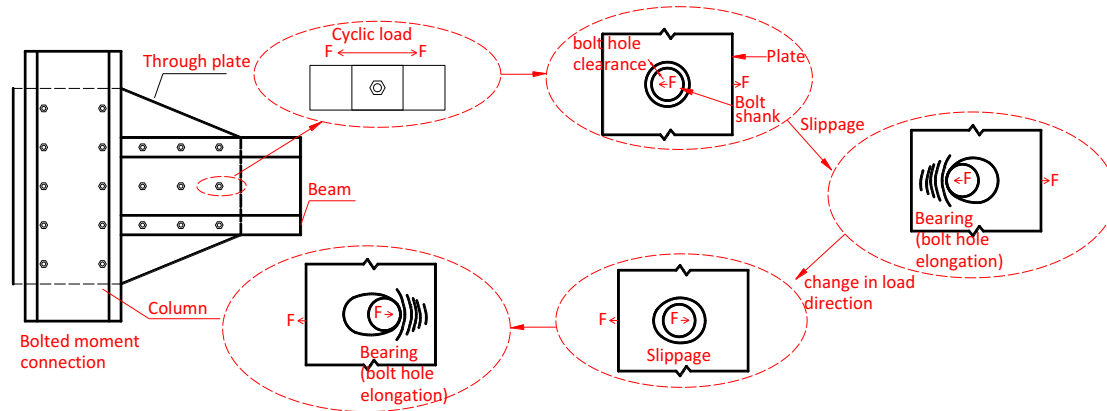


Fig. 1: Slippage and bearing behaviour of a CFS bolted moment connection with friction-slip mechanism

The monotonic and cyclic performance of CFS bolted beam-to-column connections with through plates have been the topic of several investigations before [10-16]. The results of these studies, in general, show that CFS bolted moment connections follow a typical

response comprising of a linear deformation phase followed by a slip range, a strength hardening response due to the bearing action of bolt shank against the steel sheet and finally a strength degradation phase caused by the local buckling of the connected CFS elements. It was also demonstrated that CFS moment-resisting connections are generally categorised as semi-rigid conditions [15]. Similarly, experimental tests on apex and eaves CFS bolted connections showed a semi-rigid behaviour mainly as a result of bolt-hole elongation in the thin-walled CFS plate [3]. In a follow-up study, Lim et al. [8] concluded that the bolt-group size can also considerably change the bending capacity of CFS connections. Bagheri Sabbagh et al. [17] investigated analytically the cyclic behaviour of CFS bolted moment connections by considering bolt slip effects. The results of their study showed that the proposed FE model could reasonably capture the hysteretic behaviour of the connections. However, the results were limited to the connections with curved-flange beam sections and rectangular bolt configuration. More recently, Shahini et al. [18] used experimentally validated FE models to estimate the hysteretic energy dissipation capacity of the CFS connections with circular bolting arrangement designed to slip at a specific value. It was concluded that the bolting friction-slip mechanism can effectively delay the local buckling and yielding in the CFS beams.

Based on the outcomes of the above mentioned studies, it can be concluded that the seismic performance of CFS moment-resisting connections depends on the following design parameters: (a) bolt distribution and bolt tightening (bolt slippage); (b) material yielding and bearing around the bolt holes; (c) yield lines developed in the buckled CFS plates; and (d) shape and dimensions of the beam cross section. The effects of these factors will be investigated in this study and will be used to obtain more efficient design configurations for CFS bolted moment connections with bolting friction-slip mechanism with higher energy dissipation capacity and ductility. Detailed nonlinear FE models are developed by considering the effects of initial geometrical imperfections. To model the friction-slip

mechanism, equivalent connector elements are used to represent the bearing behaviour of a single bolt against CFS plate as well as the slip action of the bolts. The developed models are then verified against the results of an experimental programme on the cyclic behaviour of CFS bolted connections [10]. Subsequently, based on a comprehensive parametric study, the influence of different design parameters such as cross-sectional shape, member classification, slip load resistance, and bolt configuration are investigated on the seismic performance of the connections. Based on the outcomes of this study, practical recommendations are proposed for more efficient design of CFS bolted moment connections with friction-slip mechanism.

2. Experimentally Validate FE models

2.1 Element type, loading and boundary conditions

Detailed Finite Element (FE) models have been shown to be efficient in predicting the monotonic [19, 20] and cyclic [17] behaviour of CFS connections. In this study, the general-purpose S8R element in ABAQUS [21] is used to model the CFS connection components. By conducting a mesh sensitivity analyses, the mesh size 20×20 mm was found to provide a balance between computational efficiency and accuracy. Fig. 2 shows the adopted boundary conditions, which are similar to the reference experimental test set-up [10]. The back-to-back channel column is connected to the base by using pinned support, while the translational degrees of freedom on top face of the column are restrained. Since the back-to-back beam was assembled with bolts and filler plates in the experimental tests, the web lines are connected together in the U_x , U_y and U_z direction using the “Tie” constraint in ABAQUS [21]. Lateral bracing in the X direction is imposed at the locations of lateral frames used in the experiments to prevent lateral torsional buckling of the beam element [10] (see Fig. 2). Previous studies showed that the panel zone deformation can also affect the rotation

of the connections [22, 23]. Due to the use of column stiffeners in the reference tests, it is assumed that the connection panel zone remains elastic.

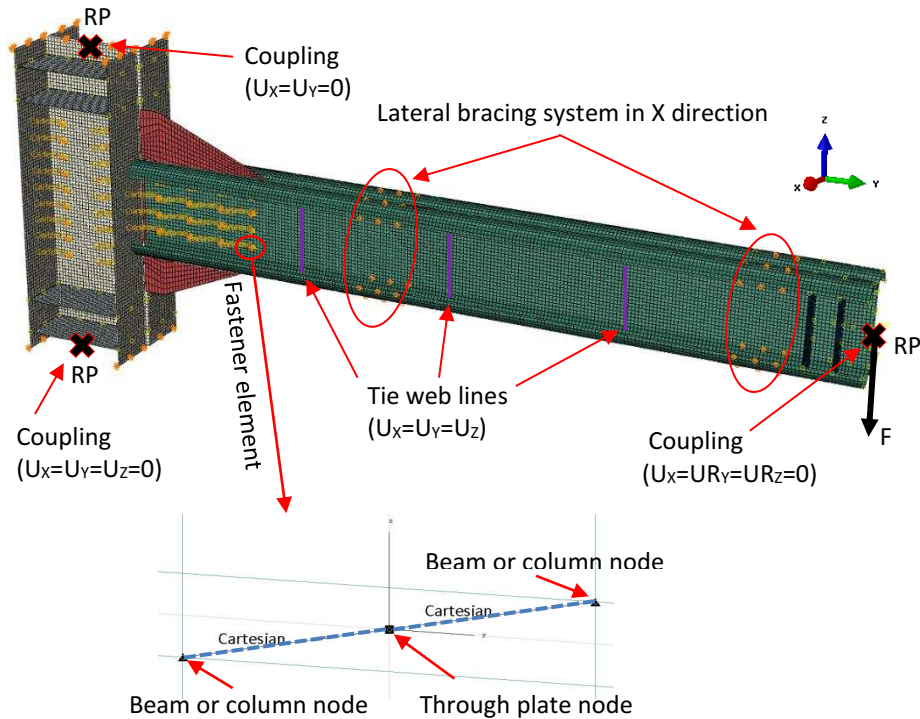


Fig. 2: FE model of the beam-column connection

A tip displacement corresponding to rotation of the connection is applied at the Reference Point (RP) on the cross-sectional centroid of the beam end section. The cyclic loading regime suggested by AISC 341-16 [24] is used as shown in Fig. 3 (similar to the reference experimental tests [10]). To obtain the response of the connections, displacement control nonlinear analyses are conducted in ABAQUS [21].

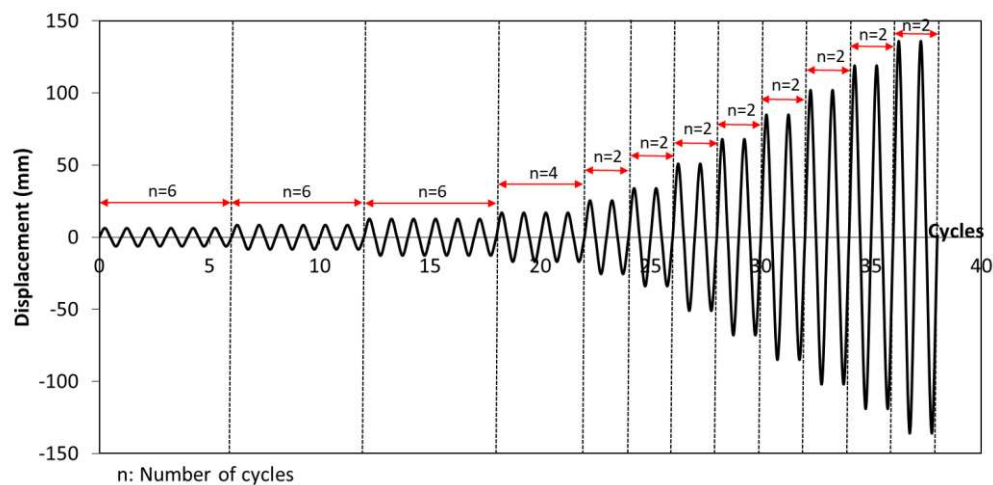


Fig. 3: Cyclic loading regime used for the reference test [10] and analytical studies

2.2 Material properties

The widely-used constitutive stress-strain model developed by Haidarali and Nethercot [25] is adopted in this study:

$$\begin{aligned}\varepsilon &= \frac{\sigma}{E} + 0.002 \left(\frac{\sigma}{\sigma_{0.2}} \right)^n && \text{for } \sigma \leq \sigma_{0.2} \\ \varepsilon &= \varepsilon_{0.2} + \frac{100(\sigma - \sigma_{0.2})}{E} && \text{for } \sigma \geq \sigma_{0.2}\end{aligned}\quad (1)$$

where E is the elastic modulus, $\sigma_{0.2}$ is the 0.2% proof stress, $\varepsilon_{0.2}$ represents the strain corresponding to $\sigma_{0.2}$, and n is a constant parameter that is used to determine the roundness of the stress-strain curve. The best agreement between the adopted model and the engineering stress-strain measurements from the coupon tests [10] is obtained by using $n = 10$, $\sigma_{0.2} = 310 \text{ MPa}$, $E = 210 \text{ GPa}$ and the ultimate strain equal to 0.08 (see Fig. 4).

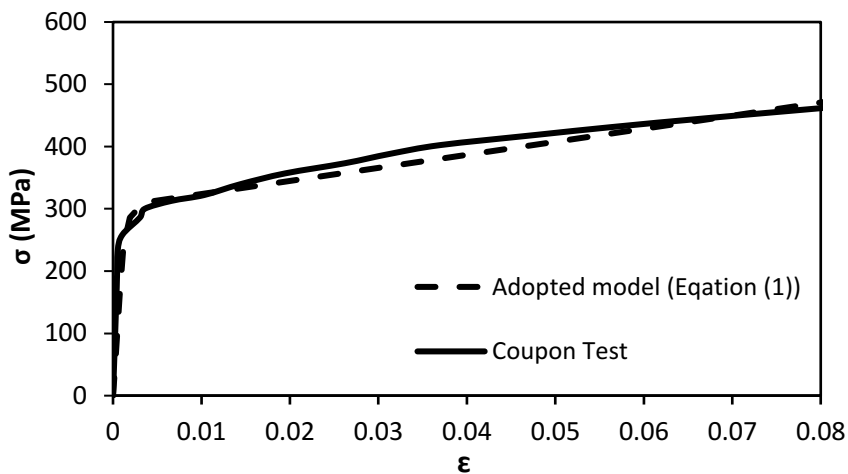


Fig. 4: Stress-strain curve used in the FE model.

2.3 Imperfection

As mentioned before, the lateral-torsional buckling was prevented in the reference tests by using a lateral bracing system in the experimental test setup [10]. Therefore, only local and distortional geometrical imperfections (the one with the lower critical buckling

resistance) are incorporated into the FE model. The imperfection magnitude for the thickness of steel sheet (t) less than 3mm is considered to be $0.94t$ and $0.34t$ for distortional and local imperfections, respectively, as suggested by Schafer and Peköz [26]. For plate thicknesses (t) grater than 3mm, the imperfection magnitude is assumed to be $0.3t\lambda_s$ as recommended by Walker [27], where λ_s is the cross-sectional slenderness. The general shape of the local and distortional imperfections is generated based on the first buckling mode of the CFS connection obtained by an eigenvalue buckling analysis in ABAQUS. It should be noted that to include geometrical imperfection under monotonic load, the eigenvalue buckling analysis is conducted by applying a tip displacement in the Z, which leads to an unsymmetrical mode as shown in Fig. 5 (a). However, in the case of cyclic loading, a symmetrical imperfection mode is generated by performing two eigenvalue buckling analyses on +Z and -Z direction and then combining the results of the first buckling mode shapes as shown in Fig. 5 (b).

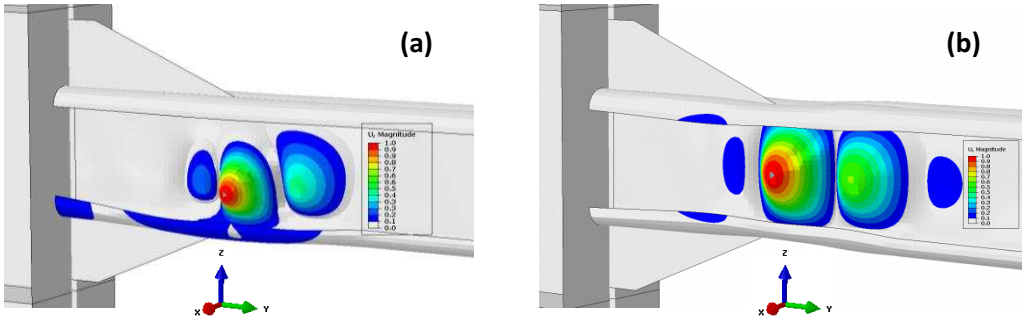


Fig. 5: Geometrical imperfection in the cases of (a) monotonic and (b) cyclic load

2.4 bolt modelling

To simulate the nonlinear behaviour of CFS connections, a simplified connection element is developed based on the concept of “component method” [28]. The bolt slip resistance F_{slip} is considered to be a function of bolt pretension force P_b (corresponding to the applied torque) and friction coefficient μ of the contact surfaces [15] :

$$F_{\text{slip}} = \mu \cdot P_b \cdot n_b \quad (2)$$

where n_b is the number of slip planes. In this study, based on the mean frictional coefficient for galvanised steel surfaces, μ is assumed to be 0.19 [29].

To model individual bolt elements, the point-based “Fastener” in ABAQUS [21] with a two-layer fastener configuration is utilised as illustrated in Fig. 2. Each layer is connected to the CFS beam element and through plate using the connector element, while the bolt shank radius is represented by defining a “physical radius” (r) to simulate the interaction between the bolt and the nodes at the bolt-hole perimeter. This modelling approach can improve the convergence of the analyses by reducing the stress concentrations at the bolt positions.

As shown in Fig. 6 (a), each fastener point is connected to the CFS steel plates through a connector element by coupling the displacement and rotation of each fastener point to those of the adjacent nodes. The friction-slip behaviour is then assigned to the connector element using “Cartesian” with three parallel translational degrees of freedom representing “Elasticity”, “Friction” and “Stop” behaviours, as shown in Fig. 6 (b). To model “Elasticity” characteristic, a rigid behaviour is assigned to the local coordinate system corresponding to the shear deformation of the bolts. The friction coefficient μ and internal contact force P_b in Eq. (2) are used to model “Friction” behaviour. The “Stop” behaviour is also used to limit the bolt slip movement within the bolt-hole clearance. The connector behaviour is schematically presented in Fig. 6 (c).

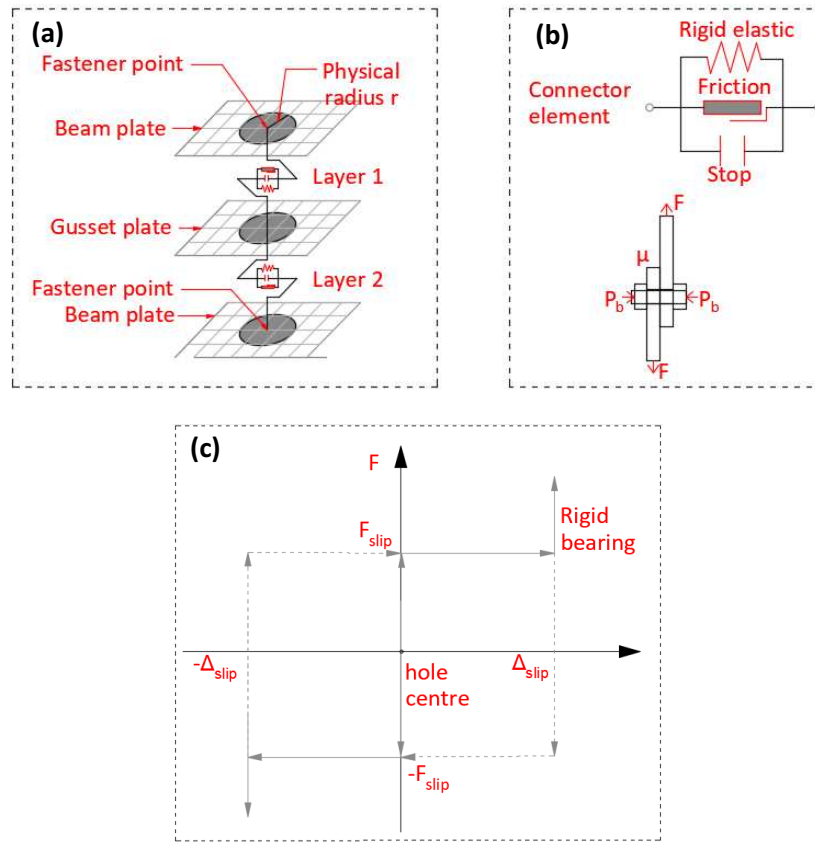


Fig. 6: Modelling of the single bolts: (a) fastener; (b) connector components; and (c) slip-bearing behaviour

Based on the above discussion, the connector behaviour is characterised as follows:

- (a) The connector is reasonably assumed to be rigid before activation of the bolt slippage (i.e. up to the slip resistance F_{slip}).
- (b) Connector shear force is gradually developed and overcomes frictional resistance (F_{slip}), and subsequently relative slippage between the two plates in each layer of the CFS connection starts to happen (see Fig. 6 (a)). The slippage will stop when the bolt shank is in contact with the hole perimeter surface.
- (c) When the relative displacement between two fastener points exceeds Δ_{slip} , the bearing stiffness is considered to be practically infinite.

2.5 Validation of FE models

The CFS bolted moment connection used in this study is mobilised with a friction-slip mechanism, which activates the bolt slippage before the buckling of CFS beam profile. Based on Eq. (2), the pretension force in the bolts is directly related to the applied torque. In the reference experimental test, the friction force was provided by pre-tensioning the connection bolts using $240\text{ N}\cdot\text{m}$ torque controlled by a torque wrench [30].

The physical radius used to model the bolts (see Fig. 6) is defined in accordance with the bolt shank radius equal to 9 mm [30]. To partially account for the effect of bolt elongation of the plate holes, the range of slippage of the stop element in Fig. 6 is increased from $\pm 1\text{mm}$ to $\pm 2\text{mm}$ in the first lines of the bolts [10]. The experimental measurements and FE responses subjected to both monotonic and cyclic loading are presented in terms of moment-rotation ($M-\Theta$) hysteretic curves in Fig. 7. The failure shape under the cyclic loads obtained from the FE model is also compared with the experimental observations in Fig. 8 at the end of cyclic loading where the rotation reaches 0.1 rad. Generally, the results of numerical simulations under cyclic load compare very well with the corresponding experimental observations. However, compared to the cyclic load condition, slightly lower strength degradation is observed in the $M-\Theta$ curve under the monotonic load. This behaviour can be attributed to the fact that the cyclic deterioration effects cannot be accurately captured under monotonic loading condition. It should be mentioned that, after a number of cycles, the slip resistance was reduced in the reference experimental test [10]. This can be justified since the high torque applied in the assembling process affects the contact surface between the plates after a number of loading cycles and the new slippage force will be then stabilised. The slippage resistance corresponding to the normal surface contact condition defined in Eq. (2) proved to be reasonable in the numerical validation of FE modelling against tested results in this study. It is shown in Fig. 8 that the detailed numerical model could accurately simulate

the bolting friction-slip mechanism and predict the general shape and location of local/distortional buckling in the tested connection.

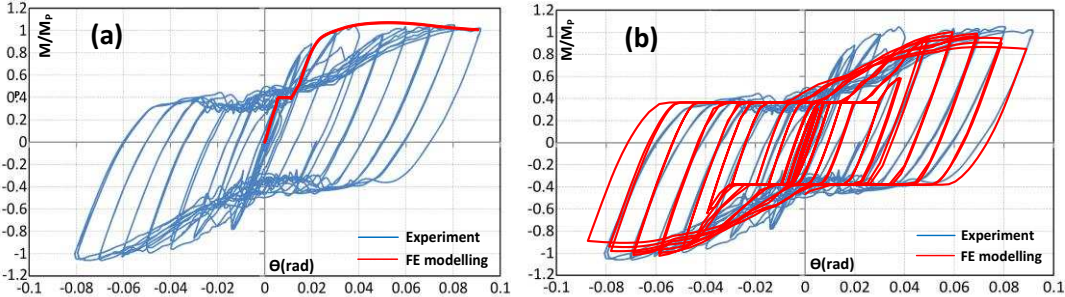


Fig. 7: Comparison between experimental (tested by Bagheri et al. [10]) and FE moment-rotation results under: (a) monotonic load and (b) cyclic load

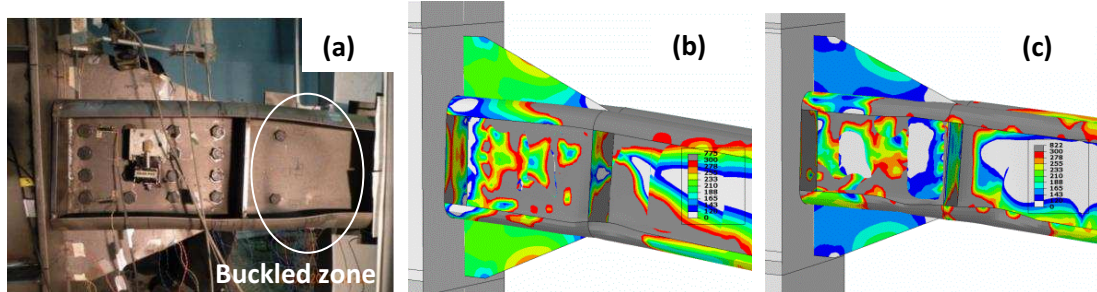


Fig. 8: Comparison between experimental observations and analytical results: (a) experimental cyclic load (adopted from [30]), (b) FE under monotonic load, and (c) FE under cyclic load

3. General response of connections with and without friction-slip mechanism

CFS bolted moment connections with bolting friction-slip mechanism can reduce damage in structural elements by absorbing a part of earthquake input energy and also decrease maximum stresses in connection zones through slippage of the bolts. To show the efficiency of the proposed system, the flexural deformation and the von-Mises stress distribution of the connections with and without bolting friction-slip mechanism are extracted from FE analysis and compared in Fig. 9. While the details of the FE models for both types of connections are similar (see Section 2), bolt slippage is prevented in the

connections with no friction-slip mechanism by using very high pretension force values [31].

The results in Fig. 9 confirm that using the proposed friction-slip mechanism can significantly reduce the stress concentrations in the connection zone.

In general, the flexural behaviours of a typical CFS bolted moment connection and the one which friction-slip mechanism is mobilised through slippage of the bolts can be distinguished in different phases as shown Fig. 10. The first phase (O-A) occurs during initial loading of the connection corresponding to the elastic performance of the connection. During this phase, the bearing action of the bolts occurs for both types of connection. However, in the connection with friction-slip the bearing action is interrupted at slip moment M_{slip} (point A), which corresponds to the beginning of bolts slippage phase. The total slippage (θ_b) in the connection can be determined based on the summation of bolt holes clearance and elongation. It will be discussed in section 4 that the slip moment (M_{slip}) and bolt clearance are the key parameters which affect the energy absorbing capability of friction-slip systems.

As can be seen in Fig. 10, point B corresponds to the position that the bearing action of the bolts is re-activated. Points C and C' show the peak moments (M_p) of the CFS bolted moment connections with and without bolting friction-slip mechanism, respectively. In the final stage, there is a sudden loss of strength for both connections due to local buckling of the beam element. In this study, it was assumed that the ultimate moment of both connections (M_u) is reached at 20% drop from peak moment (points D and D' for connections with and without friction-slip mechanism, respectively).

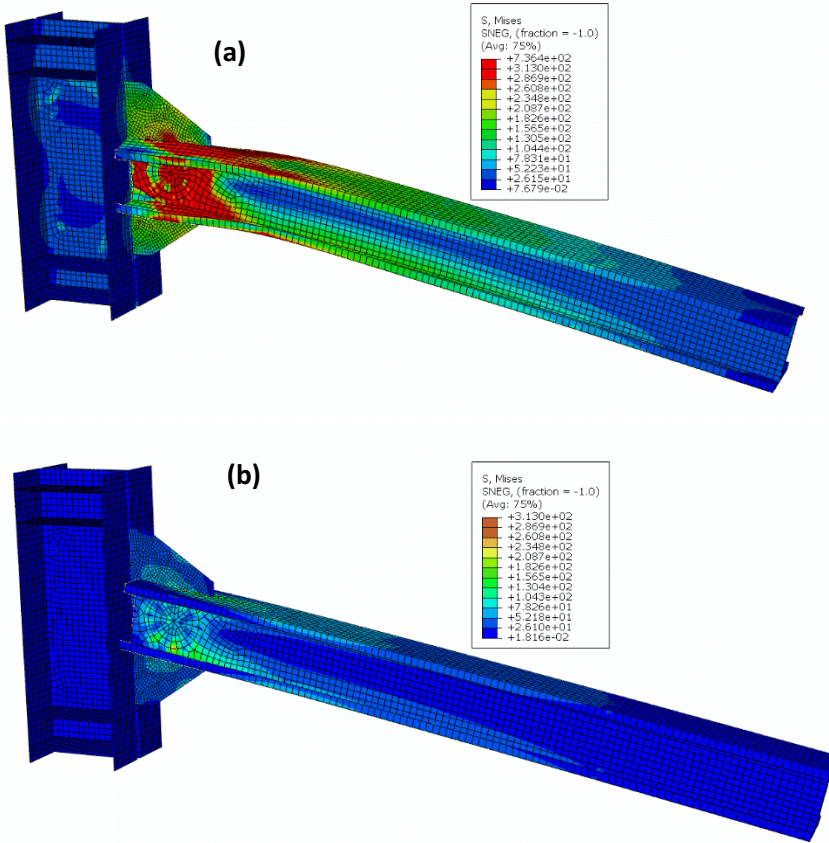


Fig. 9: Von-Mises stress distribution and coresponding damage in the (a) normal, and (b) mobilised friction-slip connections with flat-flange beam section and circular bolt configuration

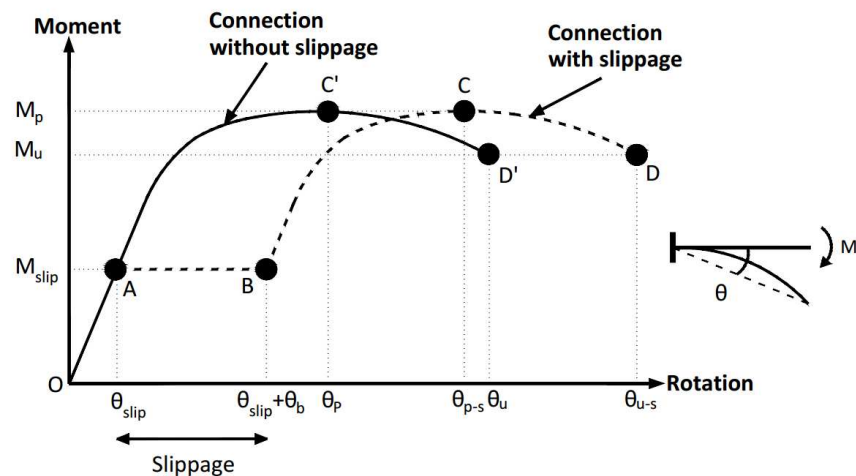


Fig. 10: Moment-rotation relationships of CFS connections with and without bolting friction-slip mechanism

Fig. 11 compares the cyclic hysteretic performance of the CFS bolted moment connection without and with friction-slip mechanism under cyclic loading regime shown in

Fig. 3. The results indicate that, similar to monotonic behaviour, using friction-slip mechanism provides a horizontal shift in each cycle of hysteretic moment-rotation curve while the peak and ultimate moments are not considerably affected. This will be discussed in more detail in the following sections.

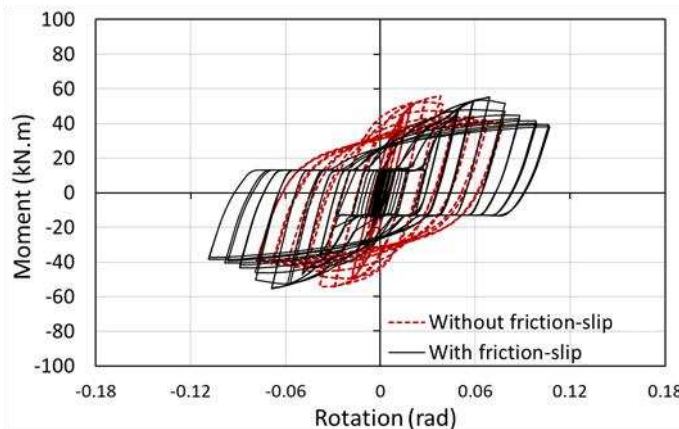


Fig. 11: Example of comparison between cyclic hysteretic performance of the CFS bolted moment connection without and with friction-slip mechanism

4. Key design parameters

In this section, the effects of key design parameters including CFS plate thickness, beam cross-sectional geometry, bolt configuration and bolt slip load resistance are investigated on the structural performance of the CFS bolted moment connections with bolting friction-slip mechanism. As shown in Table 1, four different cross-sectional shapes including flat-flange, stiffened-flange (i.e. with intermediate stiffeners), folded-flange and curved-flange are selected using 1, 2, 4, 6 mm plate thicknesses. For comparison purposes, for all cross sections the total plate width is kept constant (i.e. the same amount of material is used). For each type of connection, three different types of bolt configurations including square, diamond and circle are considered. It should be noted that, to increase the practicality of the connection, the number of bolts was reduced to 9 (compared to 16 bolts in the reference experimental tests [10]). While the circular bolt configuration may be less practical compared to the other configurations, it is used in this study mainly for comparison purposes.

Table 1: Different channel types and bolt configurations, L=2000 mm

Channel type	Bolt configuration
Flat-flange	Square
Stiffened-flange	Diamond
Folded-flange	
Curved-flange	Circle

4.1 Cross-sectional classification

Eurocode 3 (EC3) categorizes cross-sections into four different classes (1, 2, 3 and 4) according to their susceptibility to local buckling obtained based on their moment-rotation behaviour ($M-\Theta$). The EC3 classifications are illustrated in Fig. 12, where M_y , M_p and M_u represent, respectively, yield moment, plastic moment and peak moment capacity of the CFS section. Class 4 cross-sections generally experience local buckling before attaining the yield moment capacity ($M_u < M_y$). While the maximum compressive stress in class 3 cross sections reaches the yield strength, the development of full plastic moment resistance is generally prevented by local buckling of the section ($M_y < M_u < M_p$). Class 2 cross-sections

represent elements that exhibit full plastic moment capacity, but their ultimate plastic rotations are not reached due to the local plastic buckling of compression part ($M_p < M_u$). Class 1 cross-sections can reach their full plastic moment capacity with sufficient plastic rotation ($M_p < M_u$). According to the FE results, in this study all cross sectional shapes with 1, 2, 4 and 6 mm plate thickness are classified as class 4, 3, 2 and 1, respectively [31].

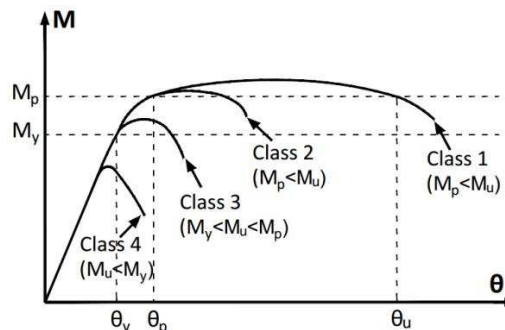


Fig. 12: EC3 cross-sectional classification definition

4.2 Effect of various bolt slip resistance

To assess the influence of using different bolt slip resistance on the overall moment-rotation behaviour of the studied connections, a range of bolt pretensions are applied on the connections with the beam flat-flange class 1 ($t=6\text{mm}$). The slip resistance design values are calculated based on the allowable slip resistance suggested by ASTM A325 [32] using the following equation:

$$R_n = 1.13 \mu N_b T_m \quad (3)$$

where R_n is slip resistance of the connection, μ is the frictional coefficient, N_b is the number of bolts, and T_m is minimum bolt pretension. Monotonic analyses are then carried out on the connections with three different bolts pretensions. Bolt pretensions are selected to be: $T_m = 90\text{ kN}$ which activates the bolt slippage while the CFS beam is still in the elastic behaviour range, $T_m = 270\text{ kN}$ which activates the slippage of the bolts when CFS is in its inelastic behaviour range, and fully clamped beam (no friction-slip). As shown in Fig. 13, the adopted friction-slip mechanism generally generates a horizontal shift in the moment-

rotation response while the global behaviour of the connection is very similar to the no slippage connection. It should be noted that, depending on bolt configuration, the behaviour of the connection with friction-slip mechanism in inelastic range (especially after buckling) may be slightly different compared to the connection with no friction-slip mechanism. It can be also seen in Fig. 13 that changing the value of the bolt pretension force can shift the starting point of slippage in moment-rotation curve while performance of the connection in both elastic and inelastic stages remains unchanged. It is worth noting that while the dominant failure mode in CFS bolted moment connection is local buckling of the beam close to bolt-group, accommodating bolting friction-slip mechanism in the connection using different bolt-pretension force and bolt configurations did not change the failure mode. Consequently, activation of friction-slip action in CFS bolted moment connections provides a means to adjust the global behaviour of the connection, especially when higher class beam sections (thicker elements) are utilised. Friction-slip mechanism and its effects on maximum moment capacity, energy dissipation and damping coefficient will be discussed in Section 5 by using the results of cyclic analyses on the connections.

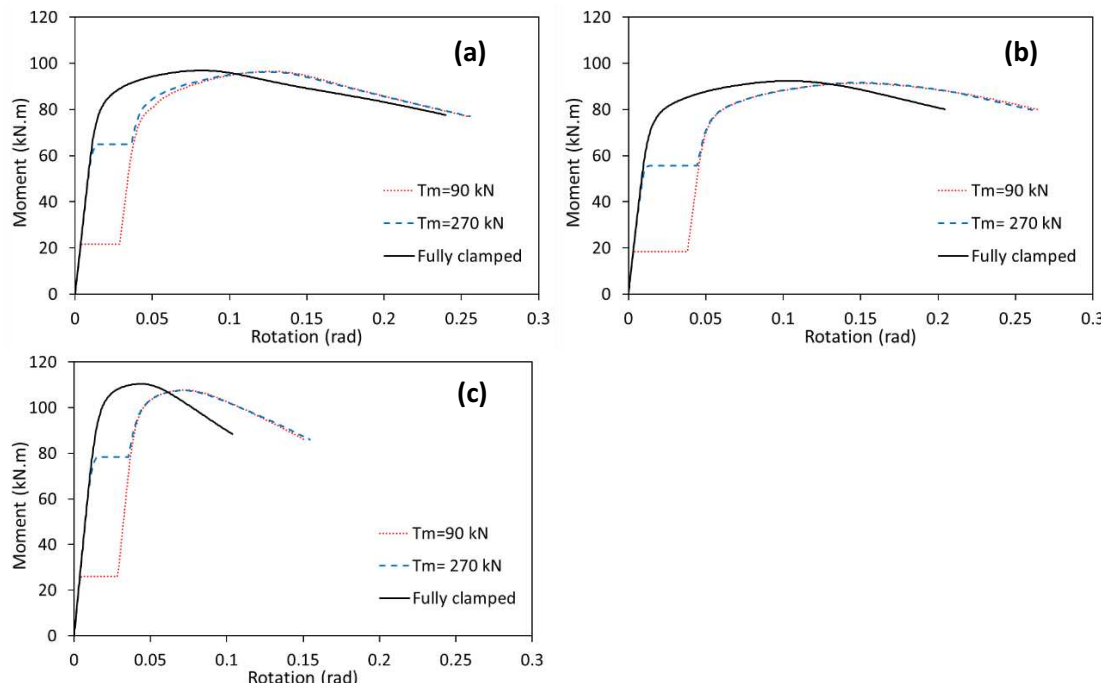
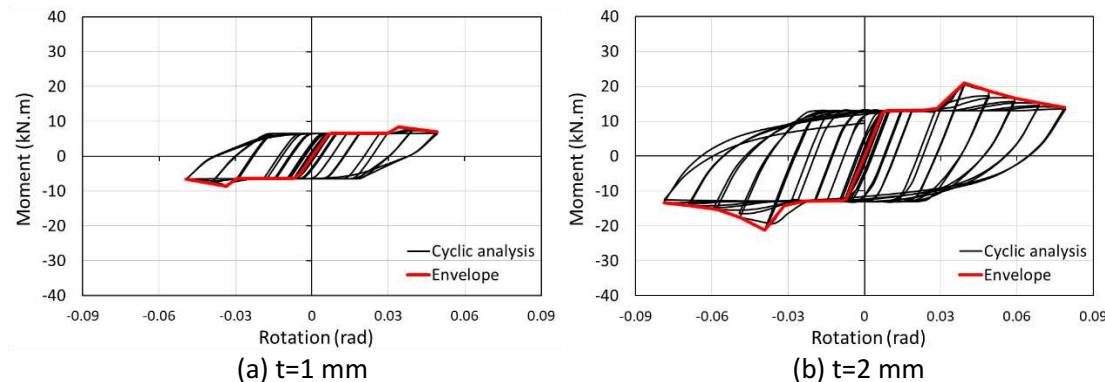


Fig. 13: The moment-rotation behaviour of class 1 connections using different bolt configurations and pretension forces: (a) Circle, (b) Diamond, (c) Square

5. Seismic Performance of CFS bolted moment connections with friction-slip mechanism

5.1 Moment-rotation behaviour

To show the typical response of CFS bolted moment connections mobilised with friction-slip system, Fig. 14 compares the moment-rotation response of the connections with flat-flange channels using 1, 2, 4 and 6 mm plate thicknesses. The moment-rotation envelope is obtained by plotting the locus of peak moment points at the first cycle of each load amplitude in both positive and negative directions. It should be mentioned that the effects of strength degradation due to cyclic loading are indirectly considered in the cyclic moment-rotation envelope (unlike monotonic moment-rotation envelope) [30, 33, 34]. In this study, the rotation of the connection is calculated by the vertical displacement at the beam tip to the length of the beam up to the through plate. It is worth mentioning that the dominant mode of failure in the selected connections with and without friction-slip is always local buckling in the CFS beam. However, the deformation of buckled area of the beam is less intensified when slip action is activated in the connection (see Fig. 9).



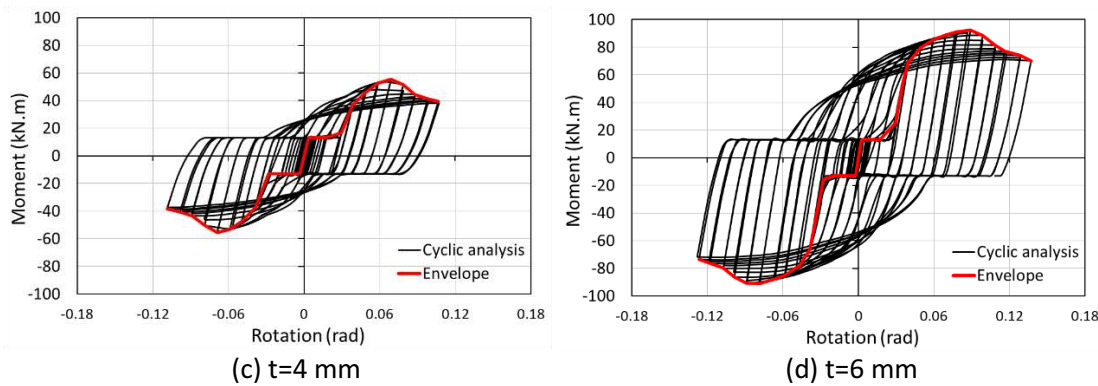


Fig. 14: Moment-rotation cyclic relationship and envelope curves of the CFS connections with flat-flange beam section and circular bolt configuration

5.2 Connection moment capacity

Fig. 15 shows the maximum moment capacity of both connections with and without bolting friction-slip system, indicating the effect of bolt slippage is generally negligible on the flexural strength of the connections regardless of the beam cross-sectional class. The minor differences can be attributed to the fact that after bolt slippage the centre of rotation shifts from the centre of the bolts, leading to a small change in the maximum flexural capacity of the connections. The results in Fig. 15 indicate that the beam cross-sectional class and the bolt configuration are the most influential parameters on the flexural capacity of the CFS connections. Compared to other bolt configurations, using a conventional square bolt configuration generally resulted in a higher (up to 32%) flexural capacity in the connections, especially where class 1 and 2 beam sections were used. While it was previously shown that bent flange sections can generally provide noticeably higher flexural capacity compared to their standard flat-flange counterparts [10, 35], the results of this study indicate that using bent flange sections can improve the capacity of the connections by less than 10%. This is referred to two main reasons: (i) effect of bi-moment generated due to presence of bolts [8], and (ii) The effect of flange shape on the moment capacity of the connection is reduced when channel sections with a deep web are utilised.

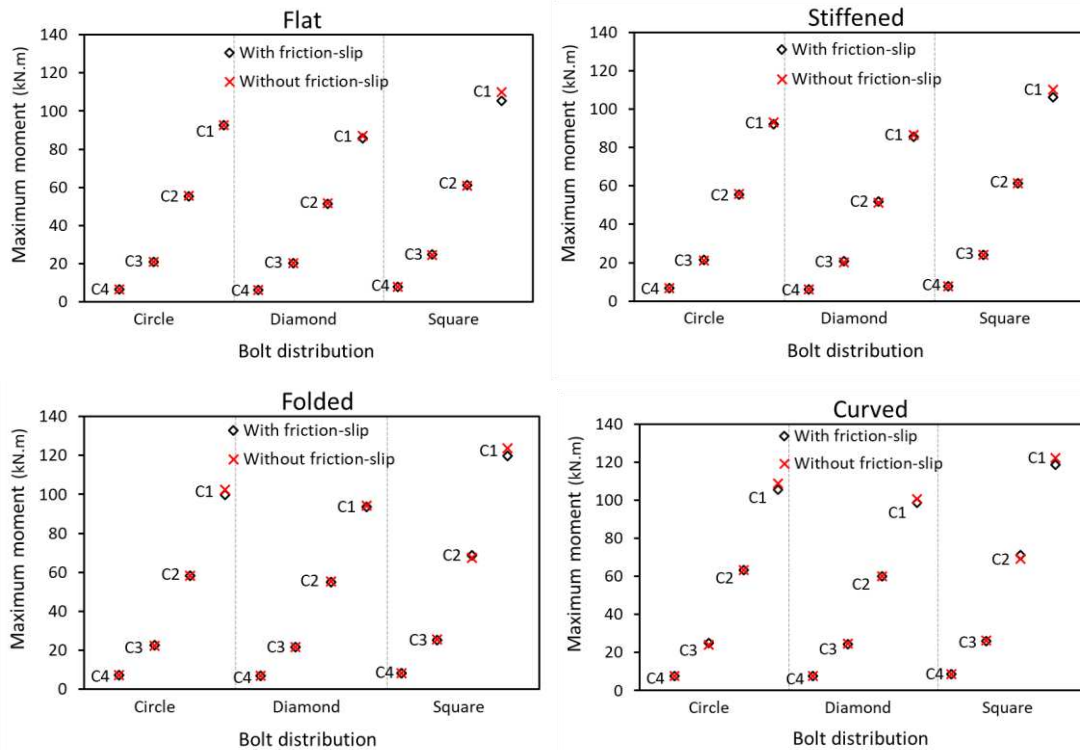


Fig. 15: Moment capacity of CFS connections with different bolt configurations and cross-section classes (C1, C2, C3, and C4 are cross-section classes 1, 2, 3 and 4, respectively)

5.3 FEMA bilinear idealisation model

To calculate the nominal yield and ultimate rotation of the connections, idealised bilinear models recommended by FEMA-356 [36] are obtained using the cyclic moment-rotation envelope results (see Section 5.1). As shown in Fig. 16, the yield rotation (θ_y) is calculated based on the condition that the secant slope intersects the actual envelope curve at 60% of the nominal yield moment (M_y), while the area under the bilinear curve is set to be equal to that enclosed by the original curve up to the target displacement (θ_t). The adopted model is suitable for CFS connections as it is capable of considering both ascending and descending post-yield responses (see Fig. 16). In this study, the rotation at which the flexural capacity of the connection reduced by 20% of its maximum value was considered as the target rotation (i.e. $\theta_t = \theta_u$) [24]. In the following sections, the FEMA idealised bilinear models calculated for the different CFS bolted moment connections are used to obtain the energy dissipation capacity and ductility of the connections under cyclic loading condition.

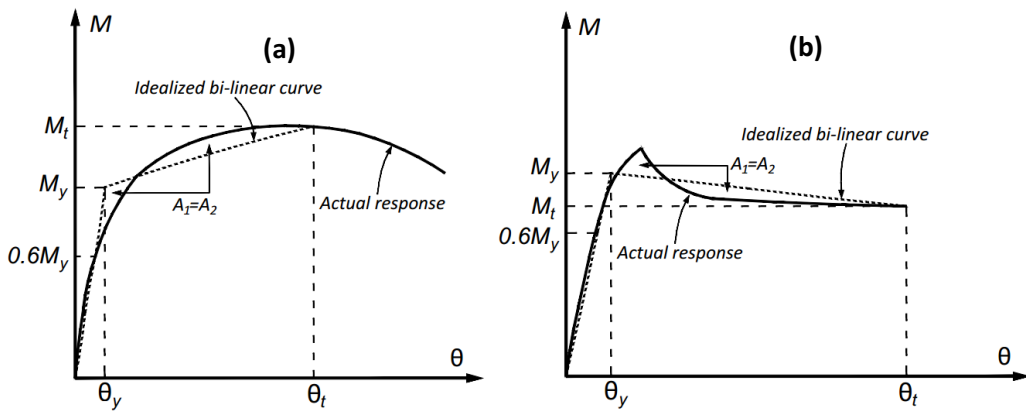


Fig. 16: FEMA idealisation model: (a) Post-yield ascending response, (b) Post-yield descending response

5.4 Energy dissipation

In this study, the area under the FEMA idealised bilinear curves (see Section 5.3) is used to calculate the energy dissipation capacity of the different CFS connections. Table 2 lists the energy dissipation capacity results without and with bolting friction-slip mechanism (stand for (E) and (E_f), respectively). It can be seen that that the energy dissipation capacity of connections with beam cross-section class 3 and 4 (2 mm and 1 mm thickness) is almost negligible due to premature buckling of the CFS beams at early stage of loading. However, class 1 and 2 elements (6 mm and 4 mm thickness) with the same cross-sectional shapes can develop their full plastic moment capacity (see section 4.1), and therefore, they result in significantly higher (up to 40 times) energy dissipation capacity in the connections.

It is shown that using bolting friction-slip mechanism can increase the energy dissipation capacity of the connections by approximately up to 200% and 50% for cross-sections class 3-4 and class 1-2, respectively. This is especially evident when diamond configuration of the bolts is used. The results indicate that in general stiffened-flange and folded-flange sections provide the highest energy dissipation capacity in the connections compared to other cross-sectional types in both connections with and without bolting friction-slip mechanism. It is also shown that the bolt distribution can play an important role in increasing the energy dissipation capacity of the connections. Using conventional square bolt configuration

generally leads to higher energy dissipation capacity (up to 25%) in the connections with beam cross-section class 3 and 4, while diamond bolt configuration usually provides higher (up to 70%) energy dissipation capacity when class 1 and 2 elements are used.

It should be noted that CFS connection with bolting friction-slip mechanism can be designed to provide higher energy dissipation by adjusting bolt pretension force in beam cross-section class 1 and 2, so slippage of the bolts is activated in the plastic stage of the moment-rotation curve. The results of this study showed that reasonable increasing of bolt holes clearance can also slightly increase the energy dissipation capacity of the connections.

Table 2: Comparison between energy dissipation capacity of the CFS bolted moment connections without (E) and with friction-slip mechanism (E_f)

Plate thickness (mm)	Beam type	Energy dissipation capacity (J)								
		Circle distribution			Diamond distribution			Square distribution		
		E	E_f	E_f/E	E	E_f	E_f/E	E	E_f	E_f/E
1	Flat	210	613	2.92	197	501	2.55	147	547	3.72
	Stiffened	407	719	1.76	308	641	2.08	371	700	1.89
	Folded	334	670	2.00	307	661	2.16	355	760	2.14
	Curved	220	559	2.54	199	564	2.83	196	610	3.11
2	Flat	478	876	1.83	393	715	1.82	294	782	2.66
	Stiffened	815	1170	1.44	615	915	1.49	741	1144	1.54
	Folded	669	1010	1.51	613	944	1.54	709	1170	1.65
	Curved	440	799	1.82	398	805	2.02	392	872	2.22
4	Flat	2441	3059	1.25	2257	2794	1.24	1930	2281	1.18
	Stiffened	3081	3812	1.24	2767	3928	1.42	2846	3474	1.22
	Folded	2686	3349	1.25	3049	3770	1.24	2998	3271	1.09
	Curved	2263	2884	1.27	2702	4094	1.52	2131	2419	1.14
6	Flat	9178	9229	1.01	7724	8776	1.14	5653	7097	1.26
	Stiffened	10298	10460	1.02	8837	10094	1.14	6517	7889	1.21
	Folded	10525	10681	1.01	11720	13278	1.13	9149	10223	1.12
	Curved	7141	7578	1.06	8256	9814	1.19	7499	7993	1.07

5.5 Damping coefficient

Damping coefficient is considered as an important indicator to evaluate the energy dissipation capability of structures [37-39]. In this study, the following equivalent viscous damping coefficient, h_e , is adopted [40-42]:

$$h_e = \frac{1}{2\pi} \frac{S_{ABC} + S_{CDA}}{S_{OBE} + S_{ODF}} \quad (4)$$

where the area of $S_{ABC} + S_{CDA}$ represents the energy dissipated in one cycle at the expected rotation (hatched area in Fig. 17). $S_{OBE} + S_{ODF}$ shows the total strain energy of the connection at the expected rotation by assuming the connection behaves elastically (double hatched area in Fig. 17). Points B and D denote, respectively, the maximum positive and negative moment capacities of a hysteresis loop. The h_e damping coefficient can demonstrate the plumpness of the hysteresis loops in non-linear systems.

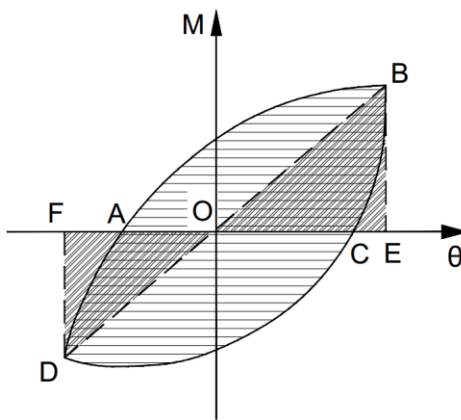


Fig. 17: Definition of the equivalent viscous damping coefficient

In this study, the equivalent viscous damping coefficients are calculated for the following two scenarios: (i) peak moment loops, in which the hysteresis loop reaches the maximum flexural capacity; (ii) ultimate moment (near-failure) loops, when the hysteresis loop reaches the ultimate point (corresponding to 20% drop from peak moment). Figs. 18 and 19 show the equivalent viscous damping coefficients at peak and ultimate moment loops, respectively, for the CFS bolted moment connections using conventional square bolt

configuration with and without friction-slip mechanism. It can be seen that the damping coefficients calculated based on the peak moment loops are smaller (up to 20 %) compared to those calculated based on the ultimate moment loops. However, in general, the results are consistent and follow a very similar trend.

It is shown in Figs. 18 and 19 that using friction-slip system in the connections with cross-sectional class 3 and 4 can significantly increase (up to 6 times) the equivalent damping coefficient of the connections, while it may cause a small reduction in the damping coefficient when cross-sections class 1 and 2 are used. The main reason for this behaviour is that the plastic moment play a more dominant role in the damping of the connection with class 1 and 2 elements, and therefore, to improve the equivalent viscous damping coefficient the activation of slip resistance has to be postponed from elastic to inelastic stage of moment-rotation curve through adjusting bolt pretension forces.

The results imply that connections with class 3 and 4 beam elements (2 mm and 1 mm thickness) without friction-slip mechanism provide very low viscous damping coefficients and, hence, may not be suitable for seismic applications. This problem can be sufficiently addressed by increasing the damping of the connections through a friction-slip mechanism (see Figs. 18 and 19). It can be also noticed that, for each type of connection, the effect of cross-sectional class on the damping coefficient is practically negligible.

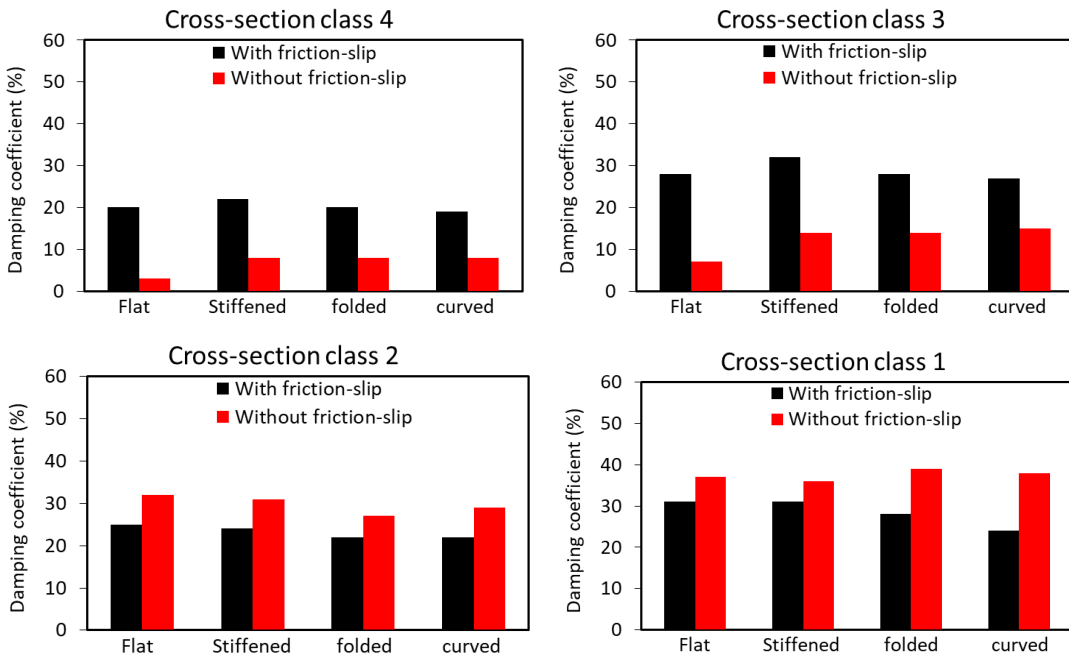


Fig. 18: Equivalent viscous damping coefficients calculated based peak moment loops

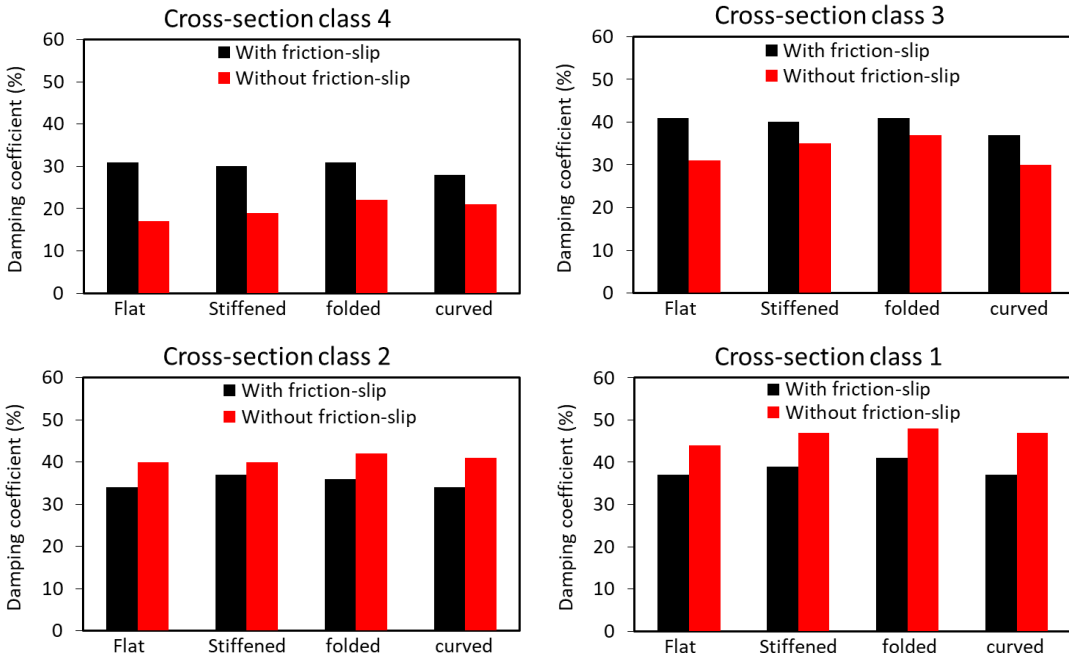


Fig. 19: Equivalent viscous damping coefficients calculated based on ultimate moment loops

5.6 Ductility ratio

According to most seismic design guidelines, moment-resisting connections in seismic regions should provide adequate ductility to resist high seismic loads. Ductility ratio (μ) is defined as the ratio of the ultimate rotation (θ_u) to the yield rotation (θ_y), as follows:

$$\mu = \theta_u / \theta_y > 1 \quad (5)$$

As mentioned before, the FEMA idealised bilinear curves developed for different CFS connections were used to estimate the ductility ratios (see Fig. 16). It should be noted that since yield rotation (θ_y) of the connections with friction-slip mechanism cannot be reasonably obtained by using FEMA idealisation model, the yield rotation is assumed to be the same as those calculated for the similar connections without friction-slip mechanism [31]. The ductility ratios of the CFS connections with and without friction-slip mechanism are compared in Fig. 20 by considering different design parameters including beam cross-sections, bolt configurations and CFS plate thicknesses. The results indicate that using bolting friction-slip mechanism is particularly more efficient for the cross-sections with lower plate thickness (i.e. class 3 and 4), where they can lead to up to 100% higher ductility ratios compared to standard bolted moment connections. This can significantly improve the seismic performance of the connections with class 3 and 4 beam sections and make them suitable for seismic applications similar to those with beam classes 1 and 2.

It can be observed from Fig. 20 that, in general, the ductility ratio of the connections is considerably influenced by the cross-sectional shape and classification of the CFS beam and the selected bolt configuration. Connections with lower beam cross-sectional class always exhibit higher ductility ratios. It can be also seen that, for the same beam cross-sectional class and bolt configuration, the highest ductility ratio is observed for folded-flange sections. For the connections with class 1 and 2 folded-flange and curved-flange sections, diamond bolt configuration leads to the highest ductility ratios. However, by using class 3 and 4 beam channels, the circle bolt configuration generally provides the highest ductility ratios. While circle and diamond bolt configurations can significantly improve (up to 85%) the ductility of the CFS moment connections with conventional square bolt configuration, they may not be very practical for the connections with a large number of bolts.

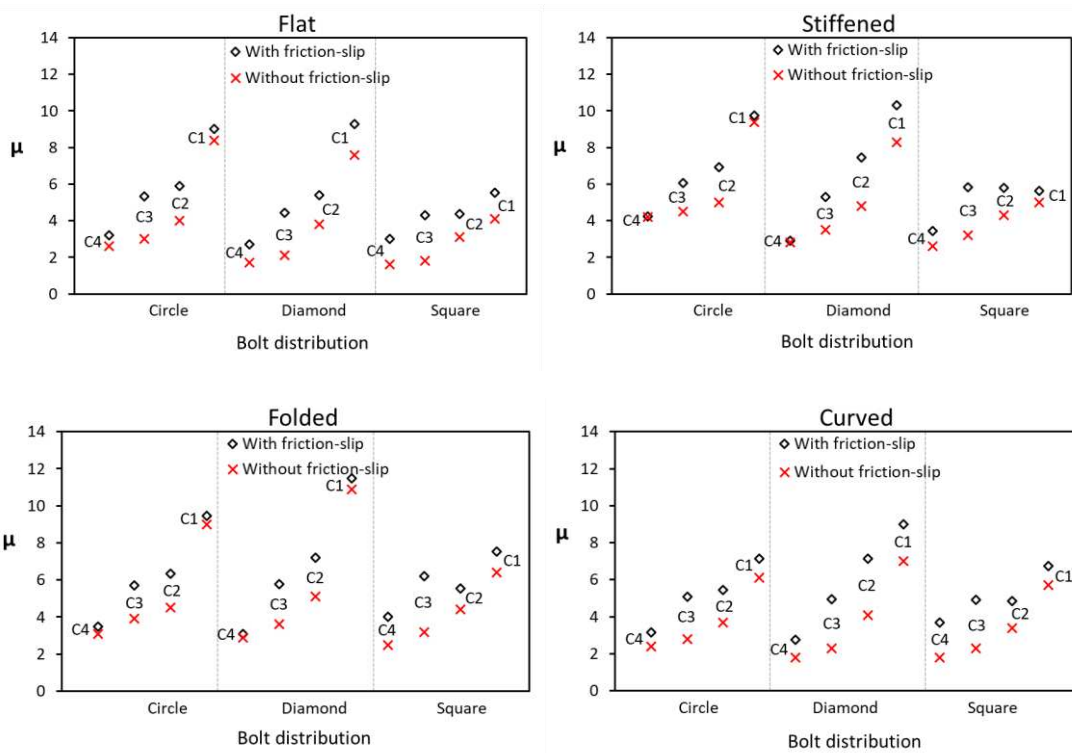


Fig. 20: Ductility ratio of CFS connections as a function of bolt configuration and beam cross-section class (C1, C2, C3, and C4 are cross-section classes 1, 2, 3 and 4, respectively)

5.7 Code requirement

Most current seismic design guidelines (e.g. AISC 341-16 [24] and Eurocode 8 [43]) categorise steel moment-resisting frames into Special Moment Frames (SMFs), Intermediate Moment Frames (IMFs), and Ordinary Moment Frames (OMFs) based on their ductility capacity. AISC 341-16 [24] suggests that SMFs, IMFs and OMFs should be capable of, respectively, exhibiting over 4%, between 2% and 4%, and less than 2% inter-storey drift with less than 20% strength degradation. In the absence of clear criteria for CFS systems, the same definitions are used in this study to assess the suitability of moment CFS connections for seismic applications. Based on the results of the cyclic moment-rotation envelope curves (see Section 5.1), Table 3 lists the AISC structural performance category of each type of connections. It is shown that some connections with beam cross sections class 4 and 3 do not satisfy SMF and IMF requirements, and therefore, cannot be used in seismic regions. However, accommodating bolting friction-slip system in these CFS bolted moment

connections can considerably improve their ductility capacity to satisfy IMF and even SMF design requirements. This conclusion is in complete agreement with the results in previous sections and highlights the efficiency of the proposed friction-slip system for CFS moment-resisting frames in seismic regions. It should be noted that in this study the effects of low cycle fatigue and fracture of steel plate under cyclic loading have not been taken into account, which can be a topic for further research in this area.

Table 3: Comparison between the structural performance of the CFS bolted moment connections with and without friction-slip mechanism according to AISC requirements

Plate thickness (mm)	Beam type	AISC requirements					
		Circle distribution		Diamond distribution		Square distribution	
		Without friction-slip	With friction-slip	Without friction-slip	With friction-slip	Without friction-slip	With friction-slip
1	Flat	OMF	IMF	OMF	IMF	OMF	IMF
	Stiffened	IMF	SMF	IMF	SMF	OMF	IMF
	Folded	IMF	SMF	IMF	SMF	OMF	SMF
	Curved	OMF	SMF	IMF	SMF	OMF	IMF
2	Flat	IMF	SMF	IMF	SMF	OMF	SMF
	Stiffened	SMF	SMF	IMF	SMF	SMF	SMF
	Folded	IMF	SMF	IMF	SMF	IMF	SMF
	Curved	IMF	SMF	IMF	SMF	IMF	SMF
4	Flat	SMF	SMF	SMF	SMF	SMF	SMF
	Stiffened	SMF	SMF	SMF	SMF	SMF	SMF
	Folded	SMF	SMF	SMF	SMF	SMF	SMF
	Curved	SMF	SMF	SMF	SMF	SMF	SMF
6	Flat	SMF	SMF	SMF	SMF	SMF	SMF
	Stiffened	SMF	SMF	SMF	SMF	SMF	SMF
	Folded	SMF	SMF	SMF	SMF	SMF	SMF
	Curved	SMF	SMF	SMF	SMF	SMF	SMF

6 Summary and conclusions

This paper aimed to investigate the efficiency of bolt friction-slip mechanism in improving the seismic performance of CFS moment-resisting connections and to provide more efficient design solutions for CFS frames in seismic regions. Experimentally validated FE models were developed by incorporating geometrical imperfections, material nonlinearity

and detailed characteristics of the bolting friction-slip system. A comprehensive analytical study was conducted to assess the influence of CFS beam cross-sectional shape and classification, bolt configuration, and slip resistance on the moment capacity, energy dissipation capacity, equivalent damping coefficient and ductility of the connections. Based on the results, the following conclusions can be drawn:

- The simplified method adopted for modelling slippage in bolted moment connection using fastener elements parallel with stop elements in ABAQUS provides an efficient and reliable tool to simulate the experimental moment-rotation behaviour and dominant failure mode of connections with friction-slip mechanism.
- Accommodating friction-slip mechanism provides a horizontal shift in the hysteretic moment-rotation response of the connections, which reduces the stress concentrations in the connection zone and postpones the failure of the CFS beam element. The effect of pretension force is generally negligible on the flexural capacity of the connections, while the bolt configuration and CFS beam cross-sectional shape and classification play the main roles. Generally using bent flange cross-section and square bolt configuration provides higher (up to 40%) flexural capacity in the connections, which is more evident in the case of higher plate thickness.
- Using bolting friction-slip mechanism can significantly improve (up to 200%) the energy dissipation capacity of the connections, especially when class 3 and 4 beams are used. Stiffened-flange and folded-flange sections generally provide the highest energy dissipation capacity, while using diamond bolt configuration can increase the energy dissipation capacity of the connections with class 1 and 2 beams by up to 70%.
- The proposed friction-slip mechanism can significantly increase (up to 6 times) the equivalent damping coefficient of the connections with class 3 and 4 beam sections, while it may cause a small reduction in the damping coefficient when cross-sections class 1 and 2 are used. This problem can be addressed by adjusting the slip resistance to be

activated in the inelastic stage of moment-rotation curve. It was also observed that the effect of cross-sectional class on the damping coefficient of the connections is practically negligible.

- The ductility of the CFS bolted moment connections can be significantly (up to 100%) increased by using friction-slip mechanism, which is particularly beneficial for cold-formed steel sections with lower plate thickness (class 3 and 4). Folded-flange sections generally resulted in the highest ductility ratios, while diamond and circle bolt configurations provided larger ductility ratios for the connections with cross-section class 1 and 2 and class 3 and 4, respectively. It was shown that conventional bolted moment connections with class 3 and 4 CFS beam sections do not generally satisfy the AISC regulations for IMF and SMF systems; however, accommodating the bolting friction-slip mechanism can improve their seismic performance to be suitable for moment-resisting frames in high seismic regions.

Acknowledgments

This work was supported by Engineering and Physical Science Research Council (EPSRC) grant EP/L019116/1. The authors would like to thank the EPSRC for providing financial supports.

References

- [1] B.W. Schafer, D. Ayhan, J. Leng, P. Liu, D. Padilla-Llano, K.D. Peterman, M. Stehman, S.G. Buonopane, M. Eatherton, R. Madsen, B. Manley, C.D. Moen, N. Nakata, C. Rogers, C. Yu, Seismic Response and Engineering of Cold-formed Steel Framed Buildings, Structures, 8, Part 2 (2016) 197-212.
- [2] L. Fiorino, O. Iuorio, R. Landolfo, Designing CFS structures: The new school bfs in naples, Thin Wall Structures, 78 (2014) 37-47.
- [3] J.B.P. Lim, D.A. Nethercot, Ultimate strength of bolted moment-connections between cold-formed steel members, Thin Wall Structures, 41 (2003) 1019-1039.
- [4] H. Moghimi, H.R. Ronagh, Performance of light-gauge cold-formed steel strap-braced stud walls subjected to cyclic loading, Engineering Structures, 31 (2009) 69-83.
- [5] S.-H. Lin, C.-L. Pan, W.-T. Hsu, Monotonic and cyclic loading tests for cold-formed steel wall frames sheathed with calcium silicate board, Thin-Walled Structures, 74 (2014) 49-58.
- [6] M. Zeynalian, H.R. Ronagh, S. Hatami, Seismic characteristics of K-braced cold-formed steel shear walls, Journal of Constructional Steel Research, 77 (2012) 23-31.

- [7] Z. Xu, Z. Chen, B.H. Osman, S. Yang, Seismic performance of high-strength lightweight foamed concrete-filled cold-formed steel shear walls, *Journal of Constructional Steel Research*, 143 (2018) 148-161.
- [8] J.B. Lim, G.J. Hancock, G.C. Clifton, C.H. Pham, R. Das, DSM for ultimate strength of bolted moment-connections between cold-formed steel channel members, *Journal of Constructional Steel Research*, 117 (2016) 196-203.
- [9] S.M. Mojtabaei, M.Z. Kabir, I. Hajirasouliha, M. Kargar, Analytical and experimental study on the seismic performance of cold-formed steel frames, *Journal of Constructional Steel Research*, 143 (2018) 18-31.
- [10] A.B. Sabbagh, M. Petkovski, K. Pilakoutas, R. Mirghaderi, Experimental work on cold-formed steel elements for earthquake resilient moment frame buildings, *Engineering Structures*, 42 (2012) 371-386.
- [11] C.M. Uang, A. Sato, J.K. Hong, K. Wood, Cyclic Testing and Modeling of Cold-Formed Steel Special Bolted Moment Frame Connections, *J Struct Eng-Asce*, 136 (2010) 953-960.
- [12] M.H. Serror, E.M. Hassan, S.A. Mourad, Experimental study on the rotation capacity of cold-formed steel beams, *Journal of Constructional Steel Research*, 121 (2016) 216-228.
- [13] Ž. Bučmys, A. Daniūnas, Analytical and experimental investigation of cold-formed steel beam-to-column bolted gusset-plate joints, *Journal of Civil Engineering and Management*, 21 (2015) 1061-1069.
- [14] J.B.P. Lim, D.A. Nethercot, Ultimate strength of bolted moment-connections between cold-formed steel members, *Thin Wall Struct*, 41 (2003) 1019-1039.
- [15] M.F. Wong, K.F. Chung, Structural behaviour of bolted moment connections in cold-formed steel beam-column sub-frames, *Journal of Constructional Steel Research*, 58 (2002) 253-274.
- [16] M.H. Serror, E.M. Hassan, S.A. Mourad, Experimental study on the rotation capacity of cold-formed steel beams, *J Constr Steel Res*, 121 (2016) 216-228.
- [17] A. Bagheri Sabbagh, M. Petkovski, K. Pilakoutas, R. Mirghaderi, Cyclic behaviour of bolted cold-formed steel moment connections: FE modelling including slip, *Journal of Constructional Steel Research*, 80 (2013) 100-108.
- [18] M. Shahini, A. Bagheri Sabbagh, P. Davidson, R. Mirghaderi, Cold-Formed Steel Bolted Moment-Resisting Connections with Friction-Slip Mechanism for Seismic Areas. CCFSS 2018, St. Louis, MO.
- [19] J.B.P. Lim, D.A. Nethercot, Finite element idealization of a cold-formed steel portal frame, *J Struct Eng-Asce*, 130 (2004) 78-94.
- [20] F. Öztürk, S. Pul, Experimental and numerical study on a full scale apex connection of cold-formed steel portal frames, *Thin-Walled Structures*, 94 (2015) 79-88.
- [21] Abaqus/CAE User's Manual, 2007, version 6.7, USA.
- [22] M. D'Aniello, R. Tartaglia, S. Costanzo, R. Landolfo, Seismic design of extended stiffened end-plate joints in the framework of Eurocodes, *Journal of Constructional Steel Research*, 128 (2017) 512-527.
- [23] R. Tartaglia, M. D'Aniello, G.A. Rassati, J.A. Swanson, R. Landolfo, Full strength extended stiffened end-plate joints: AISC vs recent European design criteria, *Engineering Structures*, 159 (2018) 155-171.
- [24] ANSI/AISC, 341-16, Seismic provisions for structural steel buildings, american institute of steel construction (AISC), (2016).
- [25] M.R. Haidarali, D.A. Nethercot, Finite element modelling of cold-formed steel beams under local buckling or combined local/distortional buckling, *Thin Wall Structures*, 49 (2011) 1554-1562.
- [26] B.W. Schafer, T. Peköz, Computational modeling of cold-formed steel: characterizing geometric imperfections and residual stresses, *Journal of Constructional Steel Research*, 47 (1998) 193-210.

- [27] A.C. Walker, Design and analysis of cold-formed sections, Halsted Press, 1975.
- [28] Eurocode 3:, design of steel structures: Part 1.1: General rules and rules for buildings, EN 1993-1-1; 2005.
- [29] Ž. Bučmys, A. Daniūnas, Analytical and experimental investigation of cold-formed steel beam-to-column bolted gusset-plate joints, Journal of Civil Engineering and Management, 21 (2015) 1061-1069.
- [30] A. Bagheri Sabbagh, Cold-formed steel elements for earthquake resistant moment frame buildings, in, PhD thesis, University of Sheffield, 2011.
- [31] J. Ye, More efficient cold-formed steel elements and bolted connections, PhD thesis, University of Sheffield; 2016.
- [32] ASTM, A325, Specification for structural joints using American Institute of Steel Construction. Chicago, Illinois, (2004).
- [33] D.A. Padilla-Llano, C.D. Moen, M.R. Eatherton, Cyclic axial response and energy dissipation of cold-formed steel framing members, Thin-Walled Structures, 78 (2014) 95-107.
- [34] D.A. Padilla-Llano, M.R. Eatherton, C.D. Moen, Cyclic flexural response and energy dissipation of cold-formed steel framing members, Thin-Walled Structures, 98 (2016) 518-532.
- [35] J. Ye, I. Hajirasouliha, J. Becque, K. Pilakoutas, Development of more efficient cold-formed steel channel sections in bending, Thin-Walled Structures, 101 (2016) 1-13.
- [36] FEMA-356. Pre standard and commentary for the seismic rehabilitation of buildings. USA, Virginia: American Society Of Civil Engineers; 2000.
- [37] A.K. Chopra, Dynamics of Structures: Theory and Applications to Earthquake Engineering, (2nd ed.)Prentice Hall, New Jersey (2001).
- [38] K.K. Wijesundara, R. Nascimbene, T.J. Sullivan, Equivalent viscous damping for steel concentrically braced frame structures. Bulletin of Earthquake Engineering 9(5) (2011) 1535-1558.
- [39] M.A. Bezabeh, S. Tesfamariam, S.F. Stiemer, Equivalent Viscous Damping for Steel Moment-Resisting Frames with Cross-Laminated Timber Infill Walls. J Struct Eng-ASCE 142(1) (2016) 1-12.
- [40] Z. Bolong, Seismic test of structure, Beijing : Earthquake Express [in chinese], (1989).
- [41] N. Yang, Y.n. Zhong, Q.t. Meng, H. Zhang, Hysteretic behaviors of cold-formed steel beam-columns with hollow rectangular section: Experimental and numerical simulations, Thin-Walled Structures, 80 (2014) 217-230.
- [42] L. Yin, G. Tang, M. Zhang, B. Wang, B. Feng, Monotonic and cyclic response of speed-lock connections with bolts in storage racks, Engineering Structures, 116 (2016) 40-55.
- [43] EN 1998-1, Design of Structures for Earthquake Resistance - Part 1: General Rules, Seismic Actions and Rules for Buildings. CEN, 2005.